Frequency Aware Face Hallucination Generative Adversarial Network with Semantic Structural Constraint

Shailza Sharma, Abhinav Dhall, and Vinay Kumar

arXiv:2110.01880v1 [cs.CV] 5 Oct 2021

***Abstract*—In this paper, we address the issue of face hallucination. Most current face hallucination methods rely on two-dimensional facial priors to generate high resolution face images from low resolution face images. These methods are only capable of assimilating global information into the generated image. Still there exist some inherent problems in these methods; such as, local features, subtle structural details and missing depth information in final output image. Present work proposes a Generative Adversarial Network (GAN) based novel progressive Face Hallucination (FH) network to address these issues present among current methods. The generator of the proposed model comprises of FH network and two sub-networks, assisting FH network to generate high resolution images. The first sub-network leverages on explicitly adding high frequency components into the model. To explicitly encode the high frequency components, an auto encoder is proposed to generate high resolution coefficients of Discrete Cosine Transform (DCT). To add three dimensional parametric information into the network, second sub-network is proposed. This network uses a shape model of 3D Morphable Models (3DMM) to add structural constraint to the FH network. Extensive experimentation results in the paper shows that the proposed model outperforms the state-of-the-art methods.**

***Index Terms*—Super Resolution, Face Hallucination, Generative Adversarial Networks, 3D Morphable Models, Discrete Cosine Transform**

I. Introduction

To obtain the high resolution image from its equivalent low resolution counterpart is referred as Super Resolution (SR). Particularly, applying super resolution on faces is known as Face Hallucination (FH). High resolution facial images are widely required in many image processing applications, such as facial emotion detection [1], pedestrian re-identification [2], facial alignment [3], face recognition [4] and face identification [5].

Based on deep learning, researchers have effectively applied numerous algorithms to solve face super resolution problem [6]. However, the first drawback of majority of these algorithms is that they rely on two dimensional facial priors to recover structural details of facial images, such as, Grm et al. [7] proposed a face Super Resolution (SR) algorithm, where the identity priors are incorporated at multiple stages of Convolutional Neural Networks (CNN) to perform image hallucination. Progressive facial attention loss is proposed by Kim et al.[8] to incorporate facial attributes in the generated SR face images. Yu et al.[9] used coarse SR image from the intermediate stage to extract heatmaps by passing that image in an UNet architecture. Extracted heatmaps are then merged with coarse SR image to generate final SR image. All the above mentioned methods used 2D priors to guide the deep learning models to generate the high resolution face images. The information extracted from the 2D priors is only capable of incorporating global features in an output image. Still the local features or the subtle structural details like skin irregularities, wrinkles and depth details are missing in the final output image. To embed the above mentioned features in the generated image, we have proposed a progressive Face Hallucination (FH) network. An auxiliary sub-network is employed in the proposed FH network by using 3D Morphable Models (3DMMs) [10] to embed structural information in the output image. 3DMMs are the three dimensional meshes of face images used to reconstruct a 3D image from its 2D counterpart using shape and texture models of Principal Component Analysis (PCA). To add the semantic structural constraint to proposed FH model, we are utilizing the PCA shape model of 3DMM [11]. The shape components of PCA shape model constitute different face parameters, like, the first shape component signifies the shape of face (slim, chubby or round etc). And the secondary shape components accounts for the more finer details (wrinkles, face irregularities, face depth etc) of face images. These three dimensional meshes with face parameters are rendered as two dimensional points on the face image. The obtained 3D points fitted on 2D images act as a target images for our auxiliary network. This auxiliary network act as a supervision network to add structural constraint to our

S. Sharma and V. Kumar are with the Department of Electronics and Communication Engineering, Thapar Institute of Engineering and Technology, India, e-mail: (ssharma_phd18@thapar.edu; vinay.kumar@thapar.edu).

A. Dhall is with Department of Human Centred Computing in Monash University, Australia, e-mail: (abhinav.dhall@monash.edu)

face hallucination network.

Second drawback of Super resolution methods based on generative adversarial networks [12], [13] is that the quantitative results produced by these methods have less values as compared to other deep learning based methods due to missing frequency details. To overcome this drawback, a sub-network comprised of an auto encoder is added along with the proposed FH network to explicitly add high frequency facial details from an face image. Discrete Cosine Transform (DCT) based feature maps with high resolution are generated using this network. Frequency domain loss is calculated between the generated DCT feature maps and ground truth DCT feature maps which is used to train the sub-network. This loss function will guide our FH network to produce output images with high quantitative values. To embed high feature DCT maps in the FH network, we used an Inverse Discrete Cosine Transform (IDCT) block. This IDCT block converts the frequency domain feature maps into the spatial domain feature maps. Then the converted feature maps are merged with the output feature maps of FH network, supervising our network to produce images with high frequency details.

Main contributions of presented work are as follows:

1) GAN based progressive face hallucination network is proposed. The generator network in the proposed network comprises of FH network and two sub-networks, assisting FH network to generate high resolution face image. The FH network consists of Hierarchical Feature Extraction Module and Computationally Efficient Channel based Attention Module. The hierarchical feature extraction module helps the model to learn hierarchical as well as primitive information present in the image. Where as channel based attention block is used to add channel-wise attention in the network and reduce the computational complexity of the network.
2) First sub-network produces high resolution DCT feature maps. This network supervises FH network to produce images with high frequency details. Proposed frequency domain based loss, assists our face hallucination network to reflect the quality of resultant images. IDCT block is used at the end of this network to convert the frequency domain feature maps to spatial domain and merge them in the FH network.
3) An auxiliary sub-network generates a high resolution 2D image with 3D parameters fitted on it. This network adds, structural constraint to our FH network, producing face images with semantic facial details, like skin irregularities, wrinkles and depth information etc.
4) Experiments on facial benchmark datasets reflect superior performance over recent state-of-the-art methods.

II. Related Work

We have discussed the framework and some recent works related to image super resolution, face hallucination and frequency domain based deep learning methods in this section. High resolution images are the most essential requirement in many computer vision applications. From the last few years, many approaches, including frequency-domain methods [2], Bayesian methods [14], [15], interpolation methods [16], regularization based methods [17], [18] and edge statistics methods [15] have been proposed for image super resolution problem. But in recent times, convolutional neural networks and generative adversarial networks have captivated extensive attention from researchers to perform the image super resolution task.

SRCNN, the first CNN based implementation was proposed by Dong et al. [19]. Based on this pioneer work, more CNN based architectures are explored for image super resolution [20], [21]. VDSR, a deep CNN architecture, based on residual learning is proposed by Kim et al. [22] to perform image super resolution. Batch Normalization layers are removed from the residual networks to increase the training accuracy of image super resolution system by Lim et al. [23]. Deep recursive network structure (DRCN) is proposed by Jiwon et al. [24] to extract feature maps repetitively from the same filter structure to reduce the count of parameters. Sometimes recursive networks induce instability in the networks due to vanishing gradient problem. Skip connections are used by the author in the SR recursive network to overcome this problem. For large upscaling factors, Lai et al.[25] proposed a deep CNN, named LapSRN, where features are upscaled using gradual upscaling technique. This network contains two branches, where first branch generate feature maps and the second branch is used for reconstruction. Residual blocks and dense blocks are combined by Zhang et al. [26] to extract the hierarchical features from each convolution layer along with the channel attention layer. For better correlation between the extracted features from the intermediate layers Dai et al. [27] proposed a network (SAN) based on second order attention mechanism. This network consists of three modules: 1) Adaptive channel-wise feature learning module, 2) NLRG- for long term memory, and 3) LSRAG- for precise feature representation.

High frequency feature extraction capability of networks is diminished by using loss functions that depend on pixel-wise differences [28]. Therefore, SRGAN [12], the first GAN based network, addresses this problem

by incorporating the loss function based on feature-wise differences. SRGAN is modified by Wang et al. [13] to generate more realistic images. The architecture integrates the dense residual blocks in the generator architecture with relativistic [29] discriminator. Feature based discriminator is proposed by Park et al. [30] which helps the model to reduce noisy artifacts and produces SR images with high structural features.

To generate a high resolution face image, Cyang et al. [31] integrated the image gradients obtained from specific face components. Edges, smooth regions and LR exemplar images, selected on the basis of pose and landmark detection constitute the face components. CNN based architecture, SICNN is proposed by Zhang et al. [29], where identity enhanced high resolution face images are generated using identity loss function. Generated SR image and HR image are applied to the face recognition CNN network and the features extracted from this network are used to calculate the identity loss function. Parsing maps and facial landmarks are used with the high resolution face images to train GAN based network for generating SR face images by Chen et al. [6].

Supervised discriminator with two inputs (SR image and the extracted features of SR image obtained from pre-trained face recognition system) is proposed by Zhang et al. [32] for face super resolution. This face super resolution system is capable of generating face images with very fine textural details. Two CNN branches- one with the facial structural information (alligned heatmaps of nose, eyes, skin and chin) and the other for the face super resolution are aggregated by Yu et al. [9]. Kalarot et al. [33] used a segmentation network to obtain three facial features: hair, skin and other parts of face. These facial feature heat maps are merged with the input image and passed to two stage image super resolution network to obtain SR images. Image SR network based on spatial attention is proposed by Chen et al. [34]. This network permit the CNN layers to learn more parameters from the high textural regions using face attention units. SRGAN [12] is improved by Wang et al. [35] by replacing the residual blocks with dense blocks for face super resolution. In addition, spectral normalization is introduced in the network to improve its training efficiency.

Discrete Cosine Transform based methods represents the feature maps in the frequency domain rather than representing them in spatial domain. For various applications, CNNs are being trained in frequency domain, such as, Zhang et al. [36] extended the idea of DCT coefficients and presented median filtering forensics approach which was based on a convolutional neural network (CNN) with an adaptive filtering layer (AFL) built in the discrete cosine transform (DCT) domain. Meanwhile, Verma et al. [37] addressed the problem of classifying images based on the number of JPEG compressions they have undergone, by utilizing deep convolutional neural networks in DCT domain. For the task of super resolution, Islam et al. [38] used directional fourier phase feature components to adaptively learn the regression kernel based on local covariance to estimate the high-resolution image. [39] presented a frequency domain neural network where convolutions in the spatial domain was cast as products in the frequency domain and nonlinearity was cast as convolution in the frequency domain. Guo et al. [40] integrated DCT into the network structure as a Convolutional DCT (CDCT) layer and formed DCT Deep SR (DCT-DSR) network.

Our approach presents a novel way to integrate spatial and frequency domain components and add structural constraint to the resultant image by using 3D parametric information. Detailed explanation of proposed methodology is present in next section.

III. Methodology

As depicted in the figure 1, generator network of the proposed architecture consist of three branches:

i) Progressive Face Hallucination Branch (PFH-B), powerfully built with a combination of cascaded hierarchical feature extraction module and channel based attention module,

ii) Semantic Structural Constraint Branch (SSC-B), serves as a supervision network by constraining PFH-B to generate resultant images with three dimensional parametric feature information, and

iii) DCT based Auto Encoder Branch (DCTAE-B), compelling PFH-B to produce images with high frequency details.

Basically, the objective of proposed face hallucination model is to find the mapping function $\mathcal{F}_{\theta_{fh}}$ (refer eq. 1) to obtain a high resolution face image (HR_{fi}) from its low resolution counterpart (LR_{fi}).

$$\mathcal{F}_{\theta_{fh}} = LR_{fi} \rightarrow HR_{fi} \tag{1}$$

where, θ_{fh} are the parameters learned throughout the mapping process. To minimize the distance between HR_{fi} and its counter LR_{fi}, proposed face hallucination network employs the combination of pixel based loss, feature based loss, structured parametric loss and DCT based loss and updates the learnable parameters during the training process. The output face images generated by face hallucination network is fed to discriminator network [12] along with the high resolution face images. In the proposed architecture, discriminator is acting as a binary classifier, and trained in such a way that it

classifies the ground-truth face images as label 1 and generated face images as label 0. On the contrary, generator is trained to trick discriminator by generating the face images similar to high resolution face images. Comprehensive training of both these networks will lead to the generation of high resolution face images.

Detailed explanation of components employed in the generator network are discussed next.

A. Progressive Face Hallucination Branch

As illustrated in figure 1, PFH-B uses a progressive upscaling technique where at every stage the input image is upscaled by the factor of 2. Further, each stage is divided into three phases. First phase is Elementary Characteristic Extraction Phase (ECE-P), where a low resolution face image is passed through a convolution layer to extract the elementary characteristics of an image. The feature maps obtained from the first phase are applied to the second phase which is Hierarchical Feature Extraction with Channel Attention Mechanism (HEF-CA). This is the most crucial component of PFH-B. HEF-CA is composed of two main blocks - Hierarchical Feature Extraction Block and Computationally Efficient Channel based Attention module, which are explained in detail in the following subsection. Output feature maps obtained from the HEF-CA are applied to the reconstruction phase, where the features maps are upsampled by the factor $\times 2$ using subpixel convolution layer [21] to get the final output image.

1) Hierarchical Feature Extraction Module: Hierarchical Feature Extraction Module (HFE-M) is shown in figure 2. Hierarchical Feature Extraction Block (HFE-B) is the building block of HFE-M. To sustain the long term memory dependency, residual connections are used between the HFE-Ms. Total five HFE-Bs are used in each HEF-CA phase, where the output feature maps of first HFE-B are applied to the second block and so on.

The motivation of Hierarchical Feature Extraction Module (HFE-M) is taken from the inception architecture [41]. As depicted in the figure 2a, the same input is applied across three different convolution layers with different kernel sizes. Notion for utilizing this complex filter structure across the input is to acquire local as well as global features of an input face image. Salient attributes like nose, eyes, lips, ears and wrinkles of face images have distinct sizes across an image. Therefore, to extract local attributes from an image, HFE-M uses convolution layers with small kernel sizes (1×1, 3×3). While the hierarchical and the global features are extracted using larger kernel sizes (5×5). Before the convolution layer with large kernel sizes (3×3, 5×5), convolution layer with 1×1 kernel size is used to curb the input channels and hence reducing the computational parameters of the architecture. All the convolution layers are followed by LeakyReLU activation function in order to introduce non-linearity in the model. The final feature maps are obtained by concatenating the individual feature maps obtained from each convolution layer with different kernel size.

2) Computationally Efficient Channel based Attention module: As depicted in figure 3, the motivation for Computationally Efficient Channel based Attention Module (CEC-AM) is taken from mobilenet V3 model [42]. Rather than using regular convolution layer, depthwise separable convolution layers (combination of depthwise convolution layer and pointwise convolution layer) are used in this block. In depthwise convolution, for each channel in the feature space a single filter is applied and followed by 1×1 convolution using pointwise convolution layer to amalgamate the feature maps of depthwise convolution layer. This layer is preferred over the regular convolution layer due to its ability to use lesser number of computational parameters without affecting the functionality of traditional convolution layer. Second fundamental component used in this module is squeeze and excitation block [43]. The essence for using this block is to explicitly model the mutuality present between the channels of convolution feature maps, guiding the network to enhance the representational quality of output features. Thus, CEC-AM is used to incline the architecture's ability to assign the accessible processing resources to the most essential information present in the input feature maps.

B. DCT based Auto Encoder Branch (DCTAE-B)

As shown in figure 1 (sub-network1), a Discrete Cosine Transform based Auto Encoder is employed in parallel with PFH-B to incorporate frequency details in our super resolution network. Basically, following two contributions are proposed in this sub-network: 1) an auto encoder is employed in parallel with PFH-B to generate high resolution DCT coefficients from low resolution DCT coefficients. 2) DCT and IDCT blocks are defined in the network to transform data from spatial domain to frequency domain and vice versa.

The autoencoder takes the DCT coefficients of LR image as input and upsample it to the DCT coefficients of HR scale. The use of skip-connections ensure long passage of information in the network. We do not use any form of normalization in the network as it tends to produce artifacts in the image. The DCT to IDCT block helps in transforming the DCT coefficients back to spatial domain, and thus provides a common link between frequency and spatial domains. The output of AE is merged with the output of PFH-B. This serves

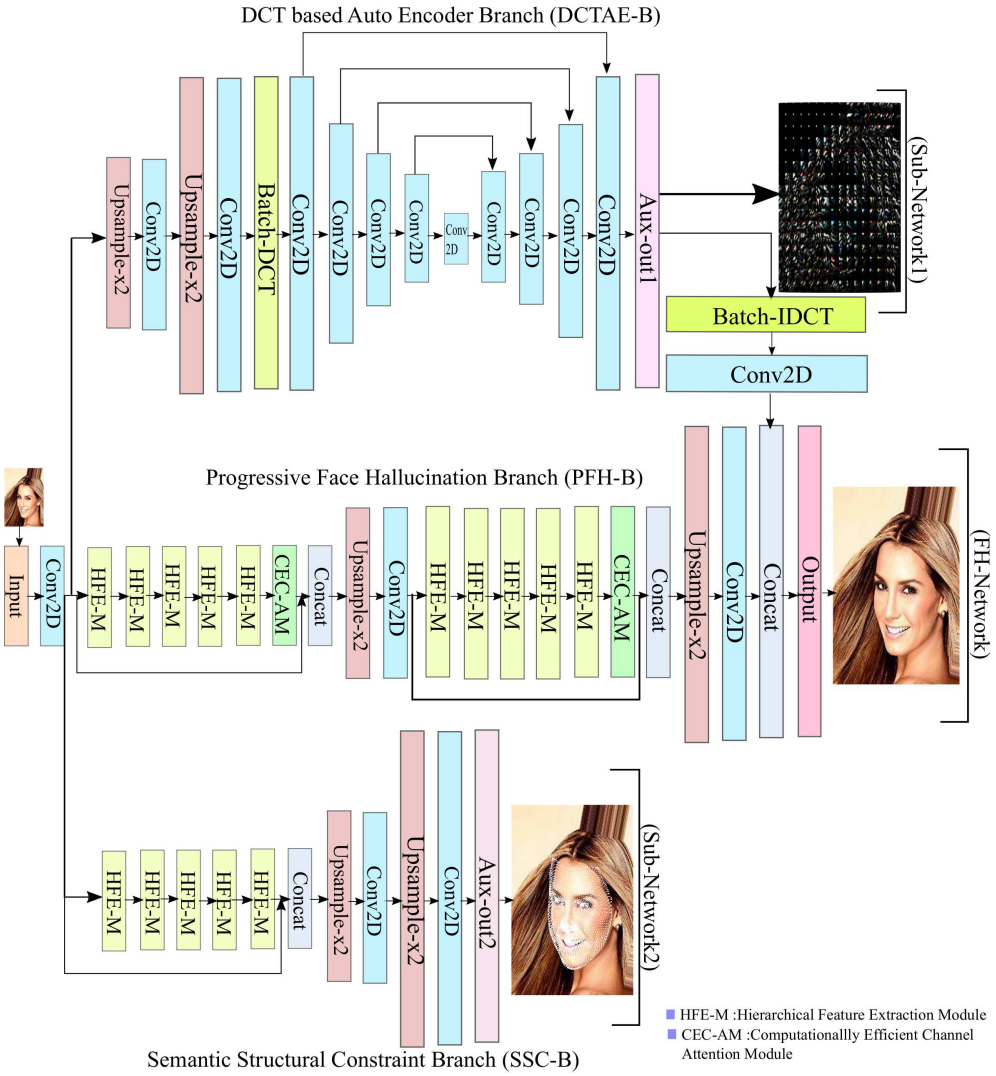


Fig. 1. Proposed Generator architecture with three branches: 1) FH network- progressive face hallucination branch from where resultant output image is generated, 2) Sub-network1- a DCT based encoder network to add high frequency components in the output image, and 3) Sub-network2- semantic structural constraint branch to add 3D parametric information in the generated image.

the purpose of using DCT coefficients which have high frequency explicitly embedded in it.

$$D_{a,b} = \frac{1}{\sqrt{2M}} \beta(a)\,\beta(b) \sum_{x=0}^{M} \sum_{y=0}^{M} i_{x,y} \cos\left[\frac{(2x+1)\,a\pi}{2M}\right] \cos\left[\frac{(2y+1)\,b\pi}{2M}\right] \tag{2}$$

1) DCT and IDCT module: To operate in the frequency domain, firstly the face images are converted from the spatial domain to frequency domain using DCT. For a single block, DCT is calculated by the formula given in equation 2 and DCT of ground-truth image is shown in figure 4

here, block size is represented by M, image is denoted by i and pixel coordinates as x and y. a and b represents indexes of spatial frequency. Scale factor β (refer eq. III-B1)is used for transform to be orthogonal.

$$\beta(v) = \begin{cases} 1/\sqrt{2}, & \text{if } v = 1. \\ 0, & \text{otherwise.} \end{cases}$$

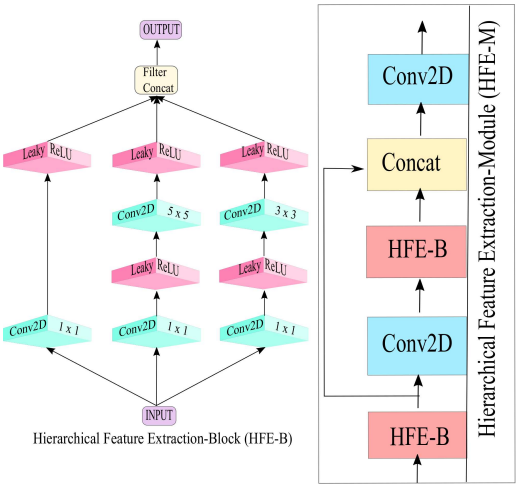


Fig. 2. Hierarchical Feature Extraction Module

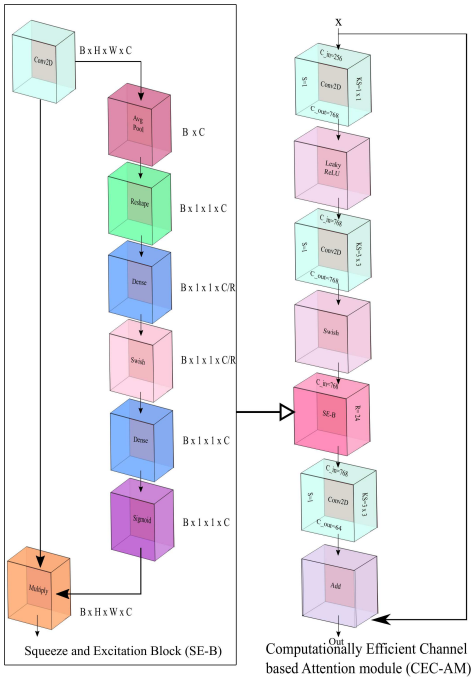


Fig. 3. Computationally Efficient Channel based Attention module

In order to establish a connection between the DCT based encoder network and main SR network, IDCT is used. IDCT transforms the frequency domain coefficients back to the spatial domain. The transformed values are then fused with the main SR network to get output images with high frequency details. The formula to calculate IDCT for single block is given by equation 3

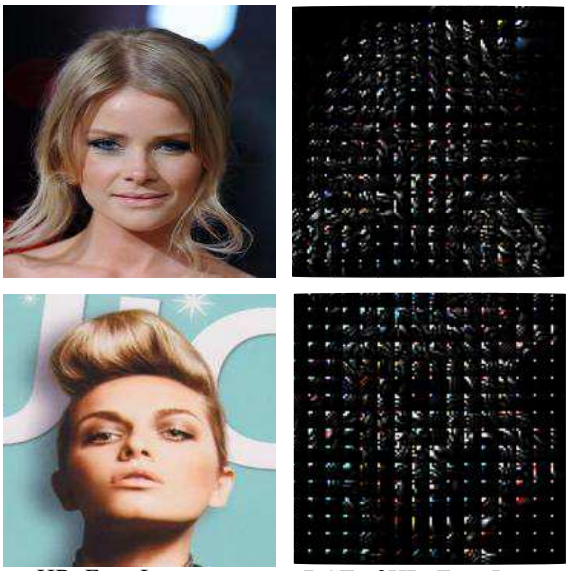


Fig. 4. Figure shows (from left to right) ground truth face image and corresponding Discrete Cosine Transform

$$i_{x,y} = \frac{1}{\sqrt{2M}} \sum_{x=0}^{M} \sum_{y=0}^{M} \beta(a)\,\beta(b)\,D_{a,b} \cos\left[\frac{(2x+1)\,a\pi}{2M}\right] \cos\left[\frac{(2y+1)\,b\pi}{2M}\right] \tag{3}$$

here, $i_{x,y}$ represents spatial domain image coefficients.

C. Semantic Structural Constraint Branch

As shown in figure 1 (subnetwork-2) is SSC-B. This auxiliary branch guides the our PFH-B to generate images with three dimensional parametric feature information. This branch consists of consecutive five HFE-Bs followed by a reconstruction module to achieve image size same as of the final output image.

To add structural semantic constraint in the proposed face super resolution, we use 3D facial parameters fitted on a 2D image. In the following subsection, we have explained the procedure to obtain the target 2D image fitted with 3D parametric information.

1) 3D model fitting to 2D images: To obtain this image following steps are followed:

1) Firstly, facial landmarks of 2D facial image are extracted through dlib library [44].
2) We used PCA shape model of Surrey Face 3D Morphable model to obtain a 3D face mesh constituting global and local face parameters . Novel



Fig. 5. Generation of training data for SSC-B. Figure shows (from left to right) a ground-truth 2D image, landmarks extraction on 2D images and then 3D parameters fitting on 2D image.

faces using PCA shape model are generated by using formula mentioned in equation 4

$$S = \bar{m} + \sum_{i}^{K} \gamma_i \sigma_i m_i \tag{4}$$

here, $\bar{m}$ - mean of example meshes,$M = [m_1, m_2, ...m_{n-1}]$ - set of principal components and K denotes the total number of scans utilized to make a model, γ - PCA shape coefficients and σ - Standard deviation

3) Using EOS library, the face mesh obtained above is fitted to the extracted landmarks [11]. Four steps are followed to perform this shape-to-landmark fitting: Estimate the pose of the facial image, shape-specific identity fitting, linear expression fitting, and contour (which includes front facial contour and occluding contour) fitting.
4) The last step is to render the obtained 3D face mesh parameters as 2D points on the face image as shown in figure 5

D. Loss Functions

To obtain the final output face image, loss function L^{fh} is optimized over M training samples. Loss Function L^{fh} is weighted combination of loss functions explained in this section.

1) DCT based loss function: For subnetwork-1 i.e. autoencoder, L_1 loss between the generated coefficients from subnetwork-1 and HR DCT coefficients of high resolution face image is calculated. This loss function as this loss function is trying to penalizes the proposed network for not predicting the high frequency details correctly. The proposed DCT based loss function ($L^{fh}_{dct/i.j}$) is defined in eq. (5)

$$L^{fh}_{dct/i.j} = \frac{1}{W_{i,j}H_{i,j}} \sum_{a=1}^{W_{i,j}} \sum_{b=1}^{H_{i,j}} | \ \Delta_{i,j}(i^{hr})_{a,b} - (SN^1_{\Theta_{g1}}(\Delta_{i,j}(i^{lr})))_{a,b} \tag{5}$$

where, W and H represents the dimensions of DCT based HR coefficients. $\Delta_{i,j}(i^{hr})$ and $\Delta_{i,j}(i^{lr})$ are the DCT coefficients extracted from the ground truth HR face image and low resolution face image, respectively. $SN^1_{\Theta_g}$represents the subnetwork-1 and its parameters.

2) Semantic Structural Constraint Loss: To add three dimensional parametric information to obtain the final output image, we proposes semantic structural constraint loss. L_1 loss is calculated between the generated image from the subnetwork-2 and its corresponding ground-truth image (2D HR face image fitted with 3D parametric information) and is given by eq. 6

$$L^{fh}_{ssc/i.j} = \frac{1}{W_{i,j}H_{i,j}} \sum_{a=1}^{W_{i,j}} \sum_{b=1}^{H_{i,j}} | \ \varsigma_{i,j}(i^{hr})_{a,b} - r (SN^2_{\Theta_{g2}}(i^{lr}))_{a,b} \tag{6}$$

here, $\varsigma_{i,j}(i^{hr})$ represents the 2D HR face image fitted with 3D parametric information. i^{lr} is the low resolution face image which is passed to subnetwork-2 ($SN^2_{\Theta_{g2}}$) to update its parameters.

3) Final loss function: Final loss function is the combination of dct based loss function, semantic structural constraint loss, feature based L_2 loss and adversarial loss. Feature based loss L^{fh}_{vgg} and adversarial losses L^{fh}_{adv} are explained it detail by Ledig et al. [12]. So, final loss function (L^{fh}) is the combination of four loss functions as mentioned in eq. 7

$$L^{fh} = L^{fh}_{vgg} + \alpha L^{fh}_{adv} + \beta L^{fh}_{dct} + \gamma L^{fh}_{ssc} \tag{7}$$

here, α, β and γ are the weight parameters used to balance the impact of individual loss functions.

IV. Experiments

A. Datasets

From CelebA dataset [45], $108,640$ images are selected for the training purpose, 5000 images for validation and 5000 for testing purpose. To validate the performance of proposed architecture, we have performed experiments on benchmark face hallucination datasets-Menpo dataset (left, right and semi-frontal profile) [46] and Helen dataset [47].

B. Implementation details

The performance evaluation for the proposed architecture is performed for upscaling factors of $\times 4$ and $\times 8$ between the high resolution face image and low resolution face image. For an upscaling factor of $\times 4$, the high resolution images are of size 128×128. These images are downsampled using bicubic kernel with a factor of $\times 4$ to generate a low resolution face images with size 32×32. For an upscaling factor of $\times 8$, the high resolution face images (128×128) are downsampled with a factor of $\times 8$ to generate low resolution images (16×16).

For every stage in progressive face hallucination branch, five HFE-Ms are used with fixed channel size (64) followed by a CEC-AM. In CEC-AM, the number of input channels are 256 and number of output channels are 64 with an expansion factor of 3. To reduce the number of parameters in fully connected layer, total channels present is a layer are divided by a factor R having value 24. The LeakyReLU hyper parameter α is 0.2. Batch size is 8; optimizer used is Adam with parameters $\beta_1 = 0.9$ and $\beta_2 = 0.999$. Initial learning rate is set to 0.0001. To minimize the distance between the high resolution face image and generated face image, l^{fh} 7 is used. To fully train the model, alternate training between the generator and discriminator is done to update their weights. Proposed model is evaluated using two commonly used metrics: SSIM (Structural Similarity Index Measurement) and PSNR (Peak Signal to Noise Ratio). For equitable comparison with the previous works, these metrics are computed on Y-channel.

C. Ablation study

In order to understand the importance of individual sub-modules of the proposed architecture, ablation study is conducted as summarized in I.

Firstly, we studied the effect of using upsampling layer at different positions in the architecture i.e. a single stage upsampling model vs a progressive stage upsampling model. From the results obtained after employing upsampling layer at end of the architecture (refer figure 6a) and at progressive stages (refer figure 6b), it is clear that multi-stage upsampling performs better than single stage upsampling model. As progressive upscaling approach allows the network to mimic the fine details present in an input image and increases its ability to learn.

The proposed architecture is compared with or without using CEC-AM. There is significant improvement in the results after adding this module in the architecture (refer figure 6b and 6c). This module is basically used to slant the network's ability to provide access of available resources to the most important information present in the feature maps.

TABLE I
CONTRIBUTION OF DIFFERENT COMPONENTS UTILIZED IN THE PROPOSED ARCHITECTURE

Components	a	b	c	d	e	f
Single stage	✓					
Multiple stages		✓	✓	✓	✓	✓
HFE-M	✓	✓	✓	✓	✓	✓
CEC-AM			✓	✓	✓	✓
Sub-network1				✓		✓
Sub-network2					✓	✓

In order to further improve the quality of the generated image, we embed sub-network1 in the architecture (refer Id). Results obtained (refer figure 6d) after adding sub-network1 in the proposed architecture supports our claim that DCT based auto encoder is able to add high frequency information in the architecture.

Still some facial details like skin irregularities and depth information is missing in the generated image. So, we tried to add these facial details using sub-network2 (refer TableIe). In this experiment we used the progressive upscaling and sub-network2 and excluded the sub-network1. Results obtained shows substantial improvement in the generated images perceptually. As facial details and skin irregularities are more prominent in these images. But there is little mismatch in the color as compare to the ground-truth images (refer figure 6e and 6g). So, for the final architecture we combined both the approaches i.e. DCT based auto encoder and 2D images with 3D parametric information to get the final output images (refer figure 6f), performs better quantitatively and qualitatively.

D. Comparison with the state-of-the-art method

We compared our proposed architecture with seven state-of-the-art methods: SRCNN [19], VDSR [22], SRGAN [12], ESRGAN [13], ImprovedFSR [35], SICNN [29], SAM3D [48] and bicubic interpolation to show the efficacy of our network. For fair comparison, we trained all these models on our training dataset with same parameters.

Menpo dataset- We evaluated the performance of our model and other state-of-the-art methods on Menpo dataset (left, right and semi-frontal profiles) [46] qualitatively and quantitatively. For left profile, our model has achieved second highest PSNR and highest SSIM for both $\times 4$ and $\times 8$ scaling factors (refer Table II). For right profile our model has achieved highest PSNR and SSIM for $\times 4$ scale. For $\times 8$ scale, our model has achieved second highest PSNR and highest SSIM values. For semi-frontal profile $\times 4$ scale, our model has second highest PSNR and highest SSIM values and highest PSNR and SSIM numbers for $\times 8$ scale.

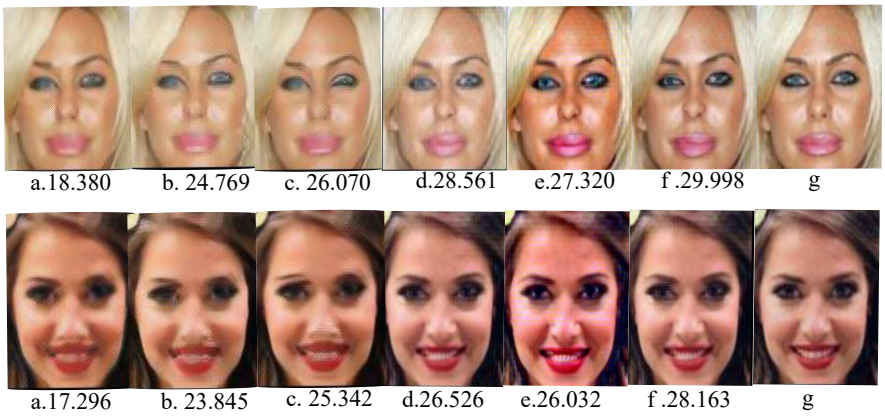


Fig. 6. Investigation of different components utilized in the proposed architecture: a) Single stage upscaling with HFE-M in generator, b) Multiscale upscaling with HFE-M, c) Adding Channel attention mechanism in b. d) Using sub-network1 (DCT based autoencoder) along with c. e) Using sub-network2 (Semantic Structural constraint block) along with c. f) Using both sub-network1 and sub-network2 along with c.

Perceptual results for Menpo dataset are represented in figures 7, 8 and 9. In figure 7, although the image generated by ImprovedFSR has highest PSNR, still there are artifacts present in the eyes and mouth region. In SAM3D model, the generated image has blemished skin with noise present in the mouth region. Only the image generated by proposed model is able to mimic the ground-truth image. As shown in figure 8, the image generated by SRGAN model has some artifacts in the hair region. And none of the competing GAN methods are able to generate a mole present on the face. Our method is recovering small details or textures present in the face image. In figure 9, competing GAN methods are unable to recover the details of the nose region. And CNN based methods are producing smooth faces with very less textural details. Image generated by our model is looking perceptually better than all other methods.

Helen dataset- For Helen test dataset [47], quantitative results (PSNR/SSIM) are shown in Table III for an upscaling factor of $\times 4$. Our method is able to achieve hightest PSNR and SSIM values as compare to state-of-the-art methods. Perceptual analysis with the PSNR and SSIM values is presented in figure 10. CNN based methods like SRCNN and VDSR are generating output images with blurriness. SRGAN and ESRGAN are also producing images with some artifacts at the eyes and cheeks. Other competing methods like ImprovedFSR and SAM3D are unable to generate better images perceptually. Only the proposed method is able to recover fine textural details like eye brows and depth details similar to the ground-truth image.

Proposed model has achieved highest SSIM and second highest PSNR for $\times 8$ factor (refer Table III). Qualitative analysis with their quantitative numbers are presented in figures 11 and 12. From the figures, it is clear that perceptually our model is performing better than the other competing methods. ImprovedFSR has highest PSNR value but visually our model is able to recover more finer details and textures.

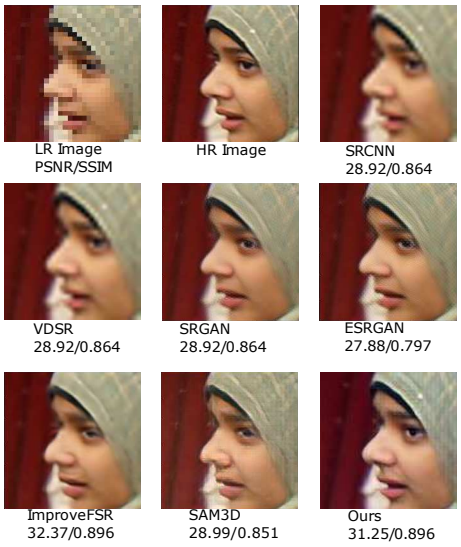


Fig. 7. Perceptual and quantitative (PSNR/SSIM) result comparison with state-of-the-art methods for the magnification factor of $\times 4$ on Menpo test dataset.

V. Conclusion

Current work presents a novel GAN based progressive face hallucination network. To generate the final output image with 3D parametric information, proposed model uses a auxiliary supervision network which is compelled to generate 2D images with 3D parametric information using shape model of 3DMM. To incorporate high frequency components in the image, an auto encoder is proposed which generates high resolution coefficients of DCT. To embed high resolution DCT information into

TABLE II
QUANTITATIVE RESULT COMPARISON ON THE BASIS OF AVERAGE PSNR (DB) AND AVERAGE SSIM ON DIFFERENT FACIAL POSES (LEFT, RIGHT AND SEMI-FRONTAL) OF MENPO DATASET.

Scale	×4						×8					
	Left		Right		Semi-frontal		Left		Right		Semi-frontal	
	PSNR	SSIM	PSNR	SSIM	PSNR	SSIM	PSNR	SSIM	PSNR	SSIM	PSNR	SSIM
Bicubic	27.32	0.794	26.28	0.772	24.89	0.763	22.01	0.634	21.07	0.602	20.31	0.501
SRCNN[19]	26.99	0.811	26.59	0.794	25.15	0.772	22.14	0.663	21.16	0.623	20.99	0.509
VDSR[22]	27.45	0.831	26.78	0.793	25.32	0.769	22.56	0.671	21.12	0.625	20.61	0.512
SRGAN[12]	29.34	0.873	29.51	0.871	28.94	0.868	22.34	0.681	22.31	0.661	21.02	0.557
ESRGAN[13]	28.99	0.821	28.83	0.813	28.43	0.813	21.04	0.662	21.06	0.621	20.19	0.532
SICNN[29]	28.09	0.812	28.12	0.803	27.02	0.799	22.45	0.679	22.69	0.659	21.21	0.613
ImprovedFSR[35]	**30.85**	0.887	30.78	0.884	**30.25**	0.877	**23.90**	0.713	**23.56**	0.676	21.28	0.623
SAM3D[48]	28.23	0.842	28.91	0.848	27.92	0.838	23.71	0.692	23.01	0.654	21.11	0.601
Ours	30.36	**0.924**	**30.81**	**0.925**	29.80	**0.922**	23.73	**0.723**	23.52	**0.689**	**21.34**	**0.641**

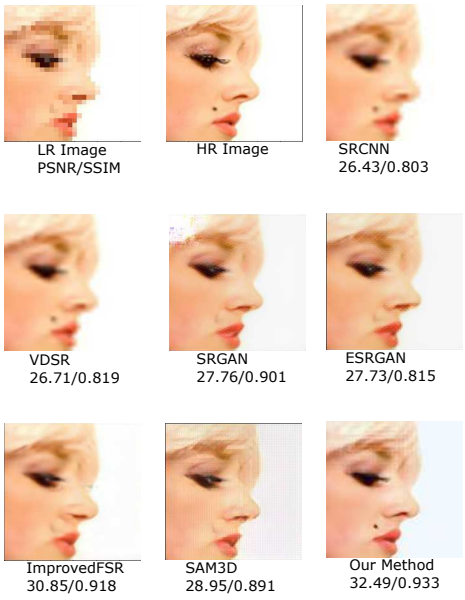


Fig. 8. Perceptual and quantitative (PSNR/SSIM) result comparison with state-of-the-art methods for the magnification factor of $\times 4$ on Menpo test dataset.

TABLE III
QUANTITATIVE RESULT COMPARISON ON THE BASIS OF AVERAGE PSNR (DB) AND AVERAGE SSIM OF HELEN DATASET.

Scale	×4		×8	
	PSNR	SSIM	PSNR	SSIM
Bicubic	25.06	0.692	21.67	0.612
SRCNN[19]	26.45	0.712	22.04	0.634
VDSR[22]	26.89	0.734	22.14	0.639
SRGAN[12]	28.45	0.851	22.31	0.689
ESRGAN[13]	27.86	0.790	21.99	0.674
SICNN[29]	26.43	0.757	22.76	0.681
ImprovedFSR[35]	28.83	0.856	**23.99**	0.701
SAM3D[48]	27.32	0.834	22.16	0.712
Ours	**28.86**	**0.911**	23.83	**0.741**

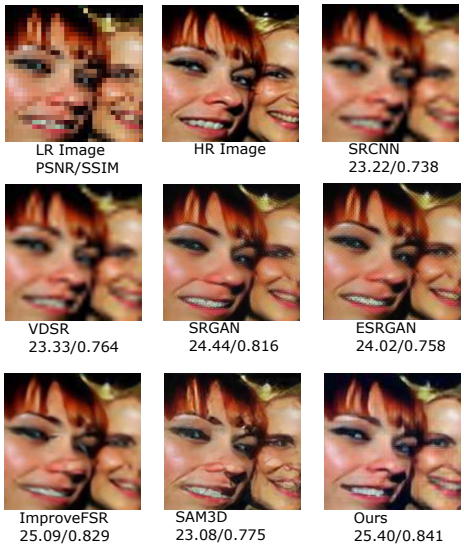


Fig. 9. Perceptual and quantitative (PSNR/SSIM) result comparison with state-of-the-art methods for the magnification factor of $\times 4$ on Menpo test dataset.

the face hallucination network IDCT block is introduced within the network to convert the frequency domain coefficients to spatial domain. Output images generated by the proposed model have subtle structural details with depth information, outperforming the state-of-the-art methods.

ACKNOWLEDGMENTS

We are greateful to Harsh Vardhan Dogra for insighful discussions.

REFERENCES

[1] C. Han, S. Shan, M. Kan, S. Wu, and X. Chen, "Face recognition with contrastive convolution," in *Proceedings of the European Conference on Computer Vision (ECCV)*, 2018, pp. 118–134.
[2] K. Nasrollahi and T. B. Moeslund, "Super-resolution: a comprehensive survey," *Machine vision and applications*, vol. 25, no. 6, pp. 1423–1468, 2014.

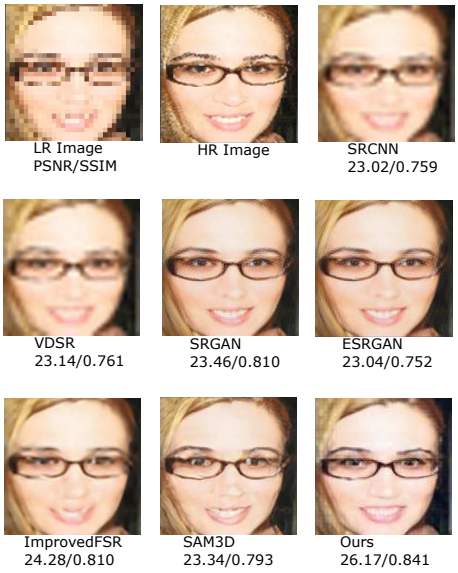


Fig. 10. Perceptual and quantitative (PSNR/SSIM) result comparison with state-of-the-art methods for the magnification factor of $\times 4$ on Helen test dataset.

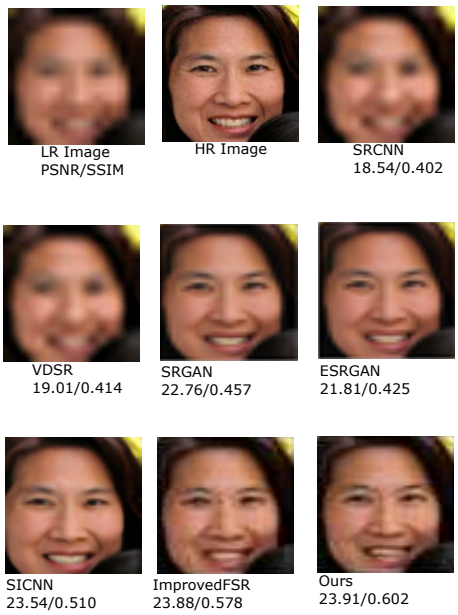


Fig. 11. Perceptual and quantitative (PSNR/SSIM) result comparison with state-of-the-art methods for the magnification factor of $\times 8$ on Helen test dataset.

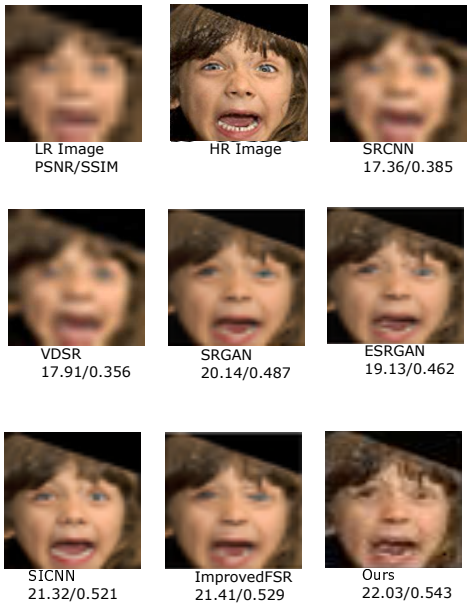


Fig. 12. Perceptual and quantitative (PSNR/SSIM) result comparison with state-of-the-art methods for the magnification factor of $\times 8$ on Helen test dataset.

[3] A. Bulat and G. Tzimiropoulos, "How far are we from solving the 2d & 3d face alignment problem?(and a dataset of 230,000 3d facial landmarks)," in *Proceedings of the IEEE International Conference on Computer Vision*, 2017, pp. 1021–1030.

[4] T. Lu, Y. Guan, Y. Zhang, S. Qu, and Z. Xiong, "Robust and efficient face recognition via low-rank supported extreme learning machine," *Multimedia Tools and Applications*, vol. 77, no. 9, pp. 11 219–11 240, 2018.

[5] Y. Taigman, M. Yang, M. Ranzato, and L. Wolf, "Deepface: Closing the gap to human-level performance in face verification," in *Proceedings of the IEEE conference on computer vision and pattern recognition*, 2014, pp. 1701–1708.

[6] Y. Chen, Y. Tai, X. Liu, C. Shen, and J. Yang, "Fsrnet: End-to-end learning face super-resolution with facial priors," in *Proceedings of the IEEE Conference on Computer Vision and Pattern Recognition*, 2018, pp. 2492–2501.

[7] K. Grm, W. J. Scheirer, and V. Štruc, "Face hallucination using cascaded super-resolution and identity priors," *IEEE Transactions on Image Processing*, vol. 29, pp. 2150–2165, 2019.

[8] D. Kim, M. Kim, G. Kwon, and D.-S. Kim, "Progressive face super-resolution via attention to facial landmark," *arXiv preprint arXiv:1908.08239*, 2019.

[9] X. Yu, B. Fernando, B. Ghanem, F. Porikli, and R. Hartley, "Face super-resolution guided by facial component heatmaps," in *Proceedings of the European Conference on Computer Vision (ECCV)*, 2018, pp. 217–233.

[10] J. Kittler, P. Huber, Z.-H. Feng, G. Hu, and W. Christmas, "3d morphable face models and their applications," in *International Conference on Articulated Motion and Deformable Objects*. Springer, 2016, pp. 185–206.

[11] P. Huber, G. Hu, R. Tena, P. Mortazavian, P. Koppen, W. J. Christmas, M. Ratsch, and J. Kittler, "A multiresolution 3d morphable face model and fitting framework," in *Proceedings of the 11th International Joint Conference on Computer Vision, Imaging and Computer Graphics Theory and Applications*, 2016.

[12] C. Ledig, L. Theis, F. Huszár, J. Caballero, A. Cunningham, A. Acosta, A. Aitken, A. Tejani, J. Totz, Z. Wang *et al.*, "Photo-realistic single image super-resolution using a generative

adversarial network," in *Proceedings of the IEEE conference on computer vision and pattern recognition*, 2017, pp. 4681–4690.

[13] X. Wang, K. Yu, S. Wu, J. Gu, Y. Liu, C. Dong, Y. Qiao, and C. Change Loy, "Esrgan: Enhanced super-resolution generative adversarial networks," in *Proceedings of the European Conference on Computer Vision (ECCV)*, 2018, pp. 0–0.

[14] J. Sun, N.-N. Zheng, H. Tao, and H.-Y. Shum, "Image hallucination with primal sketch priors," in *2003 IEEE Computer Society Conference on Computer Vision and Pattern Recognition, 2003. Proceedings.*, vol. 2. IEEE, 2003, pp. II–729.

[15] Q. Shan, Z. Li, J. Jia, and C.-K. Tang, "Fast image/video upsampling," *ACM Transactions on Graphics (TOG)*, vol. 27, no. 5, pp. 1–7, 2008.

[16] T. M. Lehmann, C. Gonner, and K. Spitzer, "Survey: Interpolation methods in medical image processing," *IEEE transactions on medical imaging*, vol. 18, no. 11, pp. 1049–1075, 1999.

[17] S. Farsiu, M. D. Robinson, M. Elad, and P. Milanfar, "Fast and robust multiframe super resolution," *IEEE transactions on image processing*, vol. 13, no. 10, pp. 1327–1344, 2004.

[18] S. P. Belekos, N. P. Galatsanos, and A. K. Katsaggelos, "Maximum a posteriori video super-resolution using a new multichannel image prior," *IEEE Transactions on Image Processing*, vol. 19, no. 6, pp. 1451–1464, 2010.

[19] C. Dong, C. C. Loy, K. He, and X. Tang, "Learning a deep convolutional network for image super-resolution," in *European conference on computer vision*. Springer, 2014, pp. 184–199.

[20] C. Dong, C. C. Loy, and X. Tang, "Accelerating the super-resolution convolutional neural network," in *European conference on computer vision*. Springer, 2016, pp. 391–407.

[21] W. Shi, J. Caballero, F. Huszár, J. Totz, A. P. Aitken, R. Bishop, D. Rueckert, and Z. Wang, "Real-time single image and video super-resolution using an efficient sub-pixel convolutional neural network," in *Proceedings of the IEEE conference on computer vision and pattern recognition*, 2016, pp. 1874–1883.

[22] J. Kim, J. K. Lee, and K. M. Lee, "Accurate image super-resolution using very deep convolutional networks," in *Proceedings of the IEEE conference on computer vision and pattern recognition*, 2016, pp. 1646–1654.

[23] B. Lim, S. Son, H. Kim, S. Nah, and K. Mu Lee, "Enhanced deep residual networks for single image super-resolution," in *Proceedings of the IEEE conference on computer vision and pattern recognition workshops*, 2017, pp. 136–144.

[24] J. Kim, J. Kwon Lee, and K. Mu Lee, "Deeply-recursive convolutional network for image super-resolution," in *Proceedings of the IEEE conference on computer vision and pattern recognition*, 2016, pp. 1637–1645.

[25] W.-S. Lai, J.-B. Huang, N. Ahuja, and M.-H. Yang, "Deep laplacian pyramid networks for fast and accurate super-resolution," in *Proceedings of the IEEE conference on computer vision and pattern recognition*, 2017, pp. 624–632.

[26] Y. Zhang, K. Li, K. Li, L. Wang, B. Zhong, and Y. Fu, "Image super-resolution using very deep residual channel attention networks," in *Proceedings of the European Conference on Computer Vision (ECCV)*, 2018, pp. 286–301.

[27] T. Dai, J. Cai, Y. Zhang, S.-T. Xia, and L. Zhang, "Second-order attention network for single image super-resolution," in *Proceedings of the IEEE conference on computer vision and pattern recognition*, 2019, pp. 11 065–11 074.

[28] J. Bruna, P. Sprechmann, and Y. LeCun, "Super-resolution with deep convolutional sufficient statistics," *arXiv preprint arXiv:1511.05666*, 2015.

[29] K. Zhang, Z. Zhang, C.-W. Cheng, W. H. Hsu, Y. Qiao, W. Liu, and T. Zhang, "Super-identity convolutional neural network for face hallucination," in *Proceedings of the European conference on computer vision (ECCV)*, 2018, pp. 183–198.

[30] S.-J. Park, H. Son, S. Cho, K.-S. Hong, and S. Lee, "Srfeat: Single image super-resolution with feature discrimination," in *Proceedings of the European Conference on Computer Vision (ECCV)*, 2018, pp. 439–455.

[31] C.-Y. Yang, S. Liu, and M.-H. Yang, "Structured face hallucination," in *Proceedings of the IEEE Conference on Computer Vision and Pattern Recognition*, 2013, pp. 1099–1106.

[32] M. Zhang and Q. Ling, "Supervised pixel-wise gan for face super-resolution," *IEEE Transactions on Multimedia*, 2020.

[33] R. Kalarot, T. Li, and F. Porikli, "Component attention guided face super-resolution network: Cagface," in *The IEEE Winter Conference on Applications of Computer Vision*, 2020, pp. 370–380.

[34] C. Chen, D. Gong, H. Wang, Z. Li, and K.-Y. K. Wong, "Learning spatial attention for face super-resolution," *IEEE Transactions on Image Processing*, vol. 30, pp. 1219–1231, 2020.

[35] M. Wang, Z. Chen, Q. J. Wu, and M. Jian, "Improved face super-resolution generative adversarial networks," *Machine Vision and Applications*, vol. 31, pp. 1–12, 2020.

[36] J. Zhang, Y. Liao, X. Zhu, H. Wang, and J. Ding, "A deep learning approach in the discrete cosine transform domain to median filtering forensics," *IEEE Signal Processing Letters*, vol. 27, pp. 276–280, 2020.

[37] V. Verma, N. Agarwal, and N. Khanna, "Dct-domain deep convolutional neural networks for multiple jpeg compression classification," *Signal Processing: Image Communication*, vol. 67, pp. 22–33, 2018.

[38] M. M. Islam, V. K. Asari, M. N. Islam, and M. A. Karim, "Single image super-resolution in frequency domain," in *2012 IEEE Southwest Symposium on Image Analysis and Interpretation*. IEEE, 2012, pp. 53–56.

[39] J. Li, S. You, and A. Robles-Kelly, "A frequency domain neural network for fast image super-resolution," in *2018 International Joint Conference on Neural Networks (IJCNN)*. IEEE, 2018, pp. 1–8.

[40] T. Guo, H. S. Mousavi, and V. Monga, "Adaptive transform domain image super-resolution via orthogonally regularized deep networks," *IEEE Transactions on Image Processing*, vol. 28, no. 9, pp. 4685–4700, 2019.

[41] C. Szegedy, W. Liu, Y. Jia, P. Sermanet, S. Reed, D. Anguelov, D. Erhan, V. Vanhoucke, and A. Rabinovich, "Going deeper with convolutions," in *Proceedings of the IEEE conference on computer vision and pattern recognition*, 2015, pp. 1–9.

[42] A. Howard, M. Sandler, G. Chu, L.-C. Chen, B. Chen, M. Tan, W. Wang, Y. Zhu, R. Pang, V. Vasudevan *et al.*, "Searching for mobilenetv3," in *Proceedings of the IEEE/CVF International Conference on Computer Vision*, 2019, pp. 1314–1324.

[43] J. Hu, L. Shen, and G. Sun, "Squeeze-and-excitation networks," in *Proceedings of the IEEE conference on computer vision and pattern recognition*, 2018, pp. 7132–7141.

[44] D. E. King, "Dlib-ml: A machine learning toolkit," *The Journal of Machine Learning Research*, vol. 10, pp. 1755–1758, 2009.

[45] Z. Liu, P. Luo, X. Wang, and X. Tang, "Deep learning face attributes in the wild," in *Proceedings of the IEEE international conference on computer vision*, 2015, pp. 3730–3738.

[46] S. Zafeiriou, G. Trigeorgis, G. Chrysos, J. Deng, and J. Shen, "The menpo facial landmark localisation challenge: A step towards the solution," in *Proceedings of the IEEE Conference on Computer Vision and Pattern Recognition Workshops*, 2017, pp. 170–179.

[47] V. Le, J. Brandt, Z. Lin, L. Bourdev, and T. S. Huang, "Interactive facial feature localization," in *European conference on computer vision*. Springer, 2012, pp. 679–692.

[48] X. Hu, W. Ren, J. LaMaster, X. Cao, X. Li, Z. Li, B. Menze, and W. Liu, "Face super-resolution guided by 3d facial priors," in *European Conference on Computer Vision*. Springer, 2020, pp. 763–780.